PROCEEDINGS OF SPIE

SPIEDigitalLibrary.org/conference-proceedings-of-spie

# Monte Carlo transmission line modelling of multilayer optical coatings for performance sensitivity of a dichroic filter for the ARIEL space telescope

Vinooja Thurairethinam, Giorgio Savini, Mario De Lucia, Gerhard Ulbricht, Gary Hawkins, et al.

Vinooja Thurairethinam, Giorgio Savini, Mario De Lucia, Gerhard Ulbricht, Gary Hawkins, Eoin Baldwin, Deirdre Coffey, Jack Piercy, Tom Ray, "Monte Carlo transmission line modelling of multilayer optical coatings for performance sensitivity of a dichroic filter for the ARIEL space telescope," Proc. SPIE 12180, Space Telescopes and Instrumentation 2022: Optical, Infrared, and Millimeter Wave, 1218048 (27 August 2022); doi: 10.1117/12.2629203

SPIE.

Event: SPIE Astronomical Telescopes + Instrumentation, 2022, Montréal, Québec, Canada

# Monte Carlo Transmission Line Modeling of Multilayer Optical Coatings for Performance Sensitivity of a Dichroic Filter for the ARIEL Space Telescope

Vinooja Thurairethinam[a], Giorgio Savini[a], Mario DeLucia[b], Gerhard Ulbricht[b], Gary Hawkins[c], Eoin Baldwin[b], Deirdre Coffey[b,d], Jack Piercy[b], and Tom Ray[b]

[a]University College London, Gower Street, London, United Kingdom
[b]Dublin Institute for Advanced Studies, 31 Fitzwilliam Place, Dublin, Ireland
[c]Infrared Multilayer Laboratory, University of Oxford, Parks Road, Oxford, United Kingdom
[d]University College Dublin, Belfield, Dublin, Ireland

## ABSTRACT

Dichroic beamsplitters, or dichroics, are filters that rely on the optical interference that occurs within thin layers to ensure the transmission and reflection of selective wavelengths of an incident beam of light. These optical components consist of a substrate coated on one or both surfaces with multiple layers of thin films, the spectral design and construction of which determine the isolation of particular wavebands. Discrepancies between the measured and expected spectral performance of optical elements with such coatings can largely be attributed to depositions errors and uncertainties in the refractive indices of the materials. Our model uses two-dimensional transmission line modeling to evaluate the transmittance of light through multilayer coatings deposited on a substrate material for given materials, angle of incidence and polarisation. This model allows us to perform Monte Carlo simulations to obtain statistical information about the tolerance of the coating performance to systematic and random uncertainties from the manufacturing process, as well as from environmental changes in space. With the aid of accurate manufacturing recipes and uncertainty amplitudes from commercial manufacturers, this tool can predict variations in the optical performance that result from the propagation of each of these uncertainties for various hypothetical scenarios. One particular application of this study are the dichroics of the ARIEL space telescope. We compare the predicted optical performance with transmission measurements at cryogenic temperatures for one of the ARIEL dichroics, which show the specification compliance of this prototype after many thermal cycles.

**Keywords:** ARIEL Space Mission, dichroic filters, dichroic tolerance, dichroic performance, optical coatings, thin film coatings, Monte Carlo simulation, systematics

## 1. INTRODUCTION

### 1.1 The ARIEL Space Mission

The Atmospheric Remote-sensing Infrared Exoplanet Large-survey (Ariel) mission has been selected as the fourth medium-class mission (M4) in ESA's Cosmic Vision program to perform spectroscopic observations of a large population of known exoplanets.[1] With an extensive statistical sample of ∼1000 planets, Ariel will move the field of planetary atmospheres beyond atmospheric characterizations of individual planets towards the overall comparative characterization of exoplanets.[2] The mission aims to spectroscopically observe its targets simultaneously in visible, NIR, and MIR wavelengths. These observations will be performed using transit, eclipse, and phase-curve spectroscopy in the 1.1-7.8 $\mu$m spectral band, along with photometry in several narrow bands in the 0.5-1.1 $\mu$m range.

The optical design of the payload is based on an off-axis Cassegrain telescope made entirely of Aluminium.[3] With the aid of several dichroic beamsplitters, the incident collimated beam from the telescope is divided into several

Further author information: (Send correspondence to V.T.)
V.T.: E-mail: vinooja.thurairethinam20@ucl.ac.uk

Space Telescopes and Instrumentation 2022: Optical, Infrared, and Millimeter Wave, edited by Laura E. Coyle, Shuji Matsuura, Marshall D. Perrin, Proc. of SPIE Vol. 12180, 1218048 · © 2022 SPIE · 0277-786X · doi: 10.1117/12.2629203

optical channels for two instruments. One of these instruments, the AIRS module, is the main spectrometer containing two channels: AIRS-Ch0 and AIRS-CH1, with resolutions of R≥100 and R≥30 and covering spectral ranges of 1.95-3.9 $\mu$m and 3.9-7.8 $\mu$m, respectively.[4] The other instrument, the Fine Guidance System (FGS) module, consists of three photometric channels and a spectrometer. FGS is an Ariel subsystem with the main purpose of ensuring the centering, focusing, and guiding of the spacecraft. Additionally, precision astrometry and photometry of the target will allow for complementary science. The requirements for these guiding and photometry specifications are achieved by defining four spectral channels from the FGS spectral bandwidth of 0.5-2.1 $\mu$m. The photometric channels are VISPhot (0.50-0.60 $\mu$m), FGS1 (0.6-0.8 $\mu$m) and FGS2 (0.8-1.1 $\mu$m). The spectrometer, NIRSpec, has a resolution of R≥15 and covers the wavelengths 1.10-1.95 $\mu$m, extended to 2.1 $\mu$m to overlap with AIRS-CH0. The channels are spatially and spectrally separated by a system of dichroics and mirrors, as shown in Fig. 1.

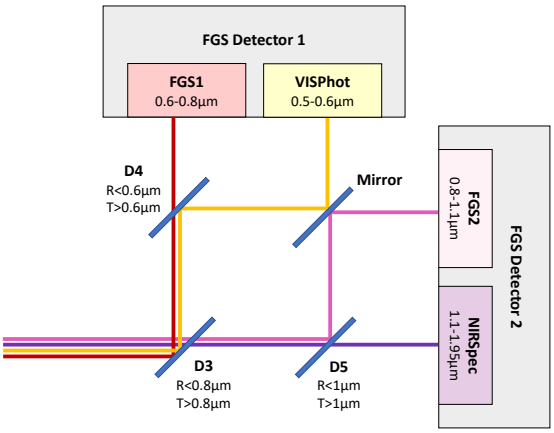


**Figure 1:** A simplified optical configuration of the FGS module portraying the concept of the dichroic and mirror system, adapted from Ref. 5

## 1.2 ARIEL D3

Infrared spectroscopy requires precise filtering to reject undesirable spectral radiation while also maximising the throughput within the required isolated passband.[6,7] Dichroic beamsplitters, or dichroics, are filters that rely on the optical interference occurring within thin-film layers to ensure the transmission and reflection of selective wavelengths from an incident light beam. Dichroics play a vital role in determining spectral response measurements. Thus, they are critical optical components for selecting and isolating wavebands for the observation of exoplanets.[8] These optical components consist of a substrate coated on one or both sides with multiple layers of thin films, whose spectral design and construction determine the isolation of particular wavebands. The precise specifications of such dichroics are adapted to satisfy spectral performance requirements. The materials that make up these filters are selected based on their non-toxicity and natural transparency within the covered wavelengths, as well as any constraints on the thicknesses of layers that may be present. Thicker layers are often subject to mechanical failure in the form of fractures during thermal cycling testing and also reduce spectral throughput through increased absorption in comparison to thinner layers.[9]

The first of the dichroics in the FGS configuration, D3, plays an essential part in the successful operation of the FGS instrument and its channels. The primary purpose of D3 is to spectrally divide the incident collimated beam from the optical path of the telescope into two spectral bands. These wavebands are isolated for two detectors within the FGS optical module in order to improve photometric accuracy. The spectral band covers the wavelength range of 0.5-2.1$\mu$m, from visible to near infra-red (NIR) wavelengths. This requires the reflection of wavelengths of 0.5-0.8$\mu$m and the transmission of the beam at wavelengths of 0.8-2.1$\mu$m. The performance of the multilayer coating of D3 ensures that these precise spectral imaging requirements are upheld while increasing

the performance sensitivity of FGS. D3 will consist of an N-BK7 substrate coated on both sides, with a broadband antireflection (AR) coating covering the rear surface of D3 to minimize ghosting reflections.

### 1.3 Modelling Multilayer Optical Coatings

Multilayer systems can be modeled using the recursive method[10] in which each layer is assumed to be homogeneous, smooth and parallel facing. As a wave of light encounters an interface of two mediums with different refractive indices, a portion of the incident is reflected when it encounters the second medium. This phenomenon occurs as the incident beam travels through the vacuum and encounters the first layer of thin film deposited on the substrate, as well as at each of the subsequent interfaces. The waves reflected at each interface differ in phase because of the time taken for the light to travel through each layer, reflect at the interface and reenter the previous medium again. This phase difference is determined by the optical thickness of each coating layer, given as the product of the physical thickness and the refractive index of the layer.[11] The amplitude of the reflection depends on the ratio of the refractive indices of the two media on either side of each interface. The electric field strength (or the amplitude reflection coefficient) is the fraction of the amplitude of the incident wave that is reflected.

For a multilayer structure, the Fresnel reflection coefficients $\rho_i$ from layer $i-1$ to layer $i$ are given by

$$\rho_i = \frac{n_{i-1} - n_i}{n_{i-1} + n_i}\,, \tag{1}$$

where $n_i$ is the refractive index of the layer $i$.

The reflection response $\Gamma_i$ at layer $i$ is initialised by $\Gamma_{N+1} = \rho_{N+1}$ for a multilayer system of $N$ layers and defined by the recursive relation

$$\Gamma_i = \frac{\rho_i + \Gamma_{i+1}\exp(-2jk_id_i)}{1 + \rho_i\Gamma_{i+1}\exp(-2jk_id_i)}, i = N, N-1, ..., 1\,, \tag{2}$$

where $k_i$ is the wavenumber and $d_i$ is the thickness of the $i^{th}$ layer, with $k_id_i$ being the phase thickness of the layer.[12] In the case of p- and s-polarized light, the refractive indices of the materials in Eq(1) are replaced by the transverse refractive indices for a given angle of incidence, $\theta$:

$$\begin{aligned} \text{s-polarisation: } & n \to n\cos(\theta) \\ \text{p-polarisation: } & n \to \frac{n}{\cos(\theta)} \end{aligned} \tag{3}$$

However, the detectors on ARIEL will respond to the intensity of the wave rather than its field amplitude.[11] The overall reflection response of the multilayer coating is given by the reflection response of the first layer, $\Gamma_1$. Following this, the fraction of the reflected incident beam is given by $|\Gamma_1|^2$. Refinement methods are frequently used to adjust the parameters, such as index of refraction and thicknesses of coating layers, of a starting design until a satisfactory performance is achieved.[13]

### 1.4 Sources of Uncertainty in Performance

The performance of the coating ensures the precise spectral imaging requirements of the dichroics are upheld, including high spectral position accuracy and environmental durability, while maximizing the performance of the filter. The design and manufacture of such a multilayer system require careful consideration of the various parameters to ensure the spectral requirements are satisfied. The selected coating materials will determine the transmission and reflection wavebands as well as the flatness of the responses across these wavelength regions.

#### 1.4.1 Manufacturing Errors

Accurate control of the thicknesses of the individual layers, as well as adequate knowledge of the refractive indices of the materials, are both critical in the successful manufacture of a multilayer coating.[14] Even seemingly minor issues in repeatability during the coating manufacture may result in a potential flight model no longer identical to its initial design. The thin-film layers of the coating are deposited onto the substrate in sequence. The coating layers frequently have optical properties that differ slightly from their bulk counterparts due to the different

columnar microstructure in thin films.[15] The effective indices of thin films produced by deposition processes may differ from those of the corresponding bulk material as a result of the microstructure of the films, which in turn, is determined by the deposition technique and conditions.[14,16] This results in anisotropy in the refractive index and manifests as a systematic error in the refractive indices, with the indices generally being smaller for thin films than for the respective bulk materials.[16] Errors within the thicknesses can stem from inaccurate termination during the deposition process of the layer.[17] This may be a direct result of insufficient sensitivity to the final thickness during the deposition of the layer or the failure to identify a fluctuation or systematic variations in the deposition conditions.[18] These complications, in turn, relate to the accuracy of the equipment used for the deposition process.

### 1.4.2 Environmental Changes in Space

Filters in a space environment are exposed to a unique set of conditions; thus, it needs to be ensured that these components can conform to such circumstances. These conditions are taken into consideration when designing a spaceflight dichroic, including the choice of materials and thickness of the component. Moreover, various tests are performed to verify the component's ability to survive in a space environment, including mechanical, physical, and thermal testing.[9] Detailed knowledge of the cryogenic performance of such filters due to the temperature-dependent spectral characteristics of the layers and substrate is necessary to produce high-performance dichroics.[19] The spacecraft module containing the payload is passively cooled to cryogenic temperatures of ∼50K to achieve the required sensitivity and stability.[20] The operation of D3 at cryogenic temperatures introduces further design constraints on the combined multilayer thicknesses and potential choices of materials that are transparent in the required waveband. Additionally, the cryogenic performance of the component is impacted by the effects of temperature on the optical constants of the materials. The refractive index of most materials is temperature-dependent, and thus, they are influenced by any offsets in the operating temperature. Furthermore, the angle of incidence of the beam arriving at an optical component is unlikely to perfectly align with the angle of incidence requirement.

## 2. METHODOLOGY

This model allows for the modeling and prediction of multilayer coating performance. A Monte Carlo (MC) simulation is performed to obtain an optimized multilayer coating design in line with the required performance of the component. A tolerance analysis of the optimized design is then conducted to study the sensitivity of the system and predict the worst offenders to the coating performance.

### 2.1 Modelling Optical Multilayer Coatings

The model calculates the overall reflectance resulting from a beam of light incident on a multilayer component at a given constant angle using Eq(1). The component comprises a substrate with N-thin film layers of specified materials and thicknesses on a single of both surfaces of the substrate. The coatings are modeled to be bounded by two semi-infinite media, the vacuum, and the substrate, and are assumed to be homogeneous and isotropic with shallow surface roughness. In the case of both a front coating, on which the light is incident, and the rear antireflection coating, which prevents ghost imaging, the performance of each coating is modeled individually. Subsequently, the reflection profile of the component, $|\Gamma_1|^2$, is attributed to the reflection of the front coating, whereas the transmissions of the two sets of coatings are combined to obtain the overall transmission profile of the component, $\tau$.

The model considers both dispersion and temperature dependence of the refractive indices of the coating and substrate through the use of wavelength and temperature-dependent expressions for the refractive indices of all materials. Dielectric losses resulting from the absorption within the multilayer coating layers and substrate were included in the model, while the bounding vacuum medium is considered to be lossless. These losses were implemented through the use of complex refractive indices taking the form of

$$n_{complex} = n_0(\lambda, T) - jk(\lambda), \tag{4}$$

where $n_0$ is the temperature and wavelength-dependent refractive index, and k is the wavelength-dependent extinction coefficient. The polarization of the incident beam may also be specified. In the case of an unpolarized input, the two spectra obtained from the p-polarized and an s-polarized cases are averaged.

### 2.1.1 Design and Optimization of Nominal Performance

This model can aid in the design of a multilayer coating component and the optimization of its performance in accordance with its specifications using an MC simulation. In principle, this model may be adapted and aid as a tool to study any given optical multilayer coating component. However, this paper will showcase its application to the ARIEL dichroic, D3, and its multilayer coating. The substrate material of D3 is known to be N-BK7. Hence, the dichroic modeled in this paper consists of a multilayer coating system with a vacuum and a semi-infinite N-BK7 substrate as the surrounding media. The collimated beam from the telescope will arrive at the dichroic at an angle of incidence of 20°, and so all calculations have been done under the assumption of a constant angle of incidence of 20°. With this, an initial design of the multilayer component is selected as a starting point supplied to the MC simulation. The spectrum resulting from this design should comply approximately with the areas of high and low transmission required by the component's specifications. Increasing the number of layers allows for a higher maximum reflection/transmission. However, the number of layers should be limited to the minimum required to obtain the desired performance. Too many coating layers may lead to complications during the manufacturing and compliance testing processes of the component, e.g., due to fracturing from internal stress or delaminating (see, e.g., Ref. 21). Hence, the number of layers of an alternating high-low index design using the same two materials was slowly increased after each optimization until an acceptable design was acquired.

The materials of the coating have not been published by the manufacturers. Therefore, $SiO_2$ and $TiO_2$ were selected as the low ($n_L \sim 1.4$) and high refractive index ($n_H \sim 2.7$) example materials due to the agreement of their transmission regions with the D3 requirements and having been used in coatings with BK7 substrates in the literature (see, e.g., Ref. 22–24). The refractive indices of the N-KB7 substrate ($n_s \sim 1.5$) and coating materials were included in the form of a Sellmeier profile as a function of temperature and wavelength. The refractive index of the substrate is modelled using the temperature-dependent Sellmeier constants provided by Ref. 25 for $50\text{K} \leq \text{T} \leq 300\text{K}$ and $0.45\mu\text{m} \leq \lambda \leq 2.7\mu\text{m}$. In the case of $TiO_2$, the temperature-dependent Sellmeier-like equation from Ref. 26 were used, where these index values have been measured within the ranges of $30°\text{C} \leq \text{T} \leq 160°\text{C}$ and $0.454\mu\text{m} \leq \lambda \leq 1.33\mu\text{m}$. Both of these models were linearly extrapolated to the required temperatures and wavelengths. Lastly, the index of refraction of $SiO_2$ was adopted from Ref. 27 in the form of a temperature-dependent Sellmeier constants for temperatures ranging from $30\text{K} \leq \text{T} \leq 310\text{K}$ at wavelengths from $0.4\mu\text{m} \leq \lambda \leq 2.6\mu\text{m}$.

The high value of refractive index contrast between the high and low-index layer materials, and thus the high ratio of impedances, allows the spectral filtering requirements to be met whilst minimizing the number of layers in order to maximize the spectral throughput.[28] This optical design of alternating low and high index layers of $SiO_2$ and $TiO_2$, respectively, results in an effective index that approximates the refractive index of the N-KB7 substrate at its front surface, thus providing a good index match. Furthermore, the extinction coefficient (k) of $TiO_2$ for the waveband considered in this paper has been shown to be negligible for thin films.[29,30] $SiO_2$ thin films have also been shown to be transparent for these wavelengths.[29,31] The majority of the absorption is expected to be accounted for by the substrate. However, N-KB7 has also been shown to be transparent in this waveband[32] and so all D3 materials can be considered to be lossless.

An initial set of estimated thicknesses of each layer is selected to provide a reasonable approximation to the required performance. These thickness parameters are optimized using the MC simulation to yield the closest acceptable approximation to the desired spectral performance. The spectral performance of the initial design is used as an attainable lower bound reference of the spectral performance. The MC simulation is then executed to randomly create slight variations in the thicknesses of a few randomly-selected layers. The goal of the simulation is to acquire a set of coating thickness parameters that will fulfill the spectral requirements of the component. In the case of D3, this target function equates to maximum reflection at $0.5 \leq \lambda \leq 0.8\mu\text{m}$ and maximum transmission at $0.8 \leq \lambda \leq 2.1\mu\text{m}$, with $0.8\mu\text{m}$ set as the transition wavelength, where the transition wavelength is defined as the wavelength at which the transmission is 50%. The sum of squared residuals between each prior spectrum and the spectral performance obtained after each MC iteration is used as a quantifying parameter to evaluate the scale of improvement in the randomly altered recipe of thicknesses. If an improvement is indeed acquired, the altered recipe is temporarily accepted and taken to be the latest reference design for the following MC iteration.

Conversely, if the recently produced design does not yield an improved spectral performance, the reference design remains unchanged, and another altered recipe is generated randomly. The thicknesses are continuously altered

in this manner until either a given number of MC iterations have been completed or the randomly obtained thicknesses generate a spectral design in agreement with the requirements of the multilayer component with no further improvements to be achieved. The number of layers was increased after each optimization with high-index material layers on both ends and an alternating high/low index materials design until an acceptable design was obtained.

## 2.2 Sources of Uncertainty

Discrepancies between the predicted and measurement performance of an optical component composed of a multilayer coating structure can be attributed to a number of uncertainties. This paper explores some of the most significant sources of uncertainty and their impact on the performance of the component. This includes uncertainties pertaining to:

a) the manufacturing process:

– uncertainties in the thicknesses of the coating layers,

– uncertainties in the refractive indices of the materials,

b) environmental changes in space:

– uncertainties in the angle of incidence of the beam,

– variation in the operating temperature of the component.

These various sources of uncertainty and their individual effect on the nominal performance of the multilayer coating are modeled. The relative changes in the performance of our multilayer design of D3 resulting from each scenario are then applied directly to the measurements of a D3 prototype performed at 4K.

### 2.2.1 Manufacturing Uncertainties

The space environment subjects coatings to a range of environmental conditions. Thus, any changes in the operating conditions of the multilayer coatings component and their impact on the performance should be considered. The cryogenic performance of the component is affected by the effects of temperature on the optical constants of the materials. The refractive index of most materials is temperature-dependent, and thus, they are influenced by any offsets in the operating temperature. The effect on the spectral performance of the multilayer structure of thermal fluctuations of the environment during operation, as well as the complete range of operating temperatures, must be considered.

Furthermore, even with seemingly perfect repeatability during manufacture, minor irreproducible variations can occur outside the parameter controls of the deposition process. These random errors in the thicknesses of the coating layers may result from the limited intrinsic precision of the deposition process, such as the consistency of optical monitoring to correctly terminate the deposition of a thin film. These unpredictable errors were simulated as random fluctuations in the form of a Gaussian distribution with a standard deviation dictated by the accuracy of the instrument and technique used for this procedure. Although this value is to be confirmed with the manufacturers of D3 in future discussions, currently, the uncertainty is approximated from the Bühler IBS 1600 tool, which is able to deposit coatings with a uniformity of $\pm 0.5\%$.[33] This value has been used as no better reproducibility information is available to us. The deviation of the spectral performance from the nominal performance of the multilayer system as a result of this error was found. This process is repeated 10,000 times for each wavelength, and a spectrum is computed each time to obtain a distribution of these deviations as a function of the wavelength of light. This allowed us to examine the wavelengths and layers that are most sensitive to these manufacturing uncertainties, as well as the potential value that a range of discrepancies will generate due to random errors.

The temperature-dependent models used in this paper for N-KB7 and $SiO_2$ have been stated to have measurement uncertainties of $\pm 2 \times 10^{-4}$ and $\pm 1 \times 10^{-5}$, respectively.[25,27] However, the refractive index model of $TiO_2$ was linearly extrapolated to temperatures much further outside of the temperatures applicable to the model. Therefore, for the work described here, a scenario of a systematic error of -0.1% was considered for the index of $TiO_2$.

### 2.2.2 Environmental Changes in Space

Changes in the environment during operation in space for a spaceflight multilayer coating component can significantly impact the nominal spectral performance. Temperature fluctuations of approximately ±0.5K are expected to occur during the course of an ARIEL observation.[34] This shift in temperature from the average operating temperature of 47.5K results in a variation in the refractive indices of the D3 materials due to their temperature dependence. The effect on the spectral performance of the multilayer structure of thermal fluctuations of the environment during operation, as well as the complete range of the expected operating temperatures of 35-60K during the mission, was simulated.

Moreover, despite the beam incident on the dichroic being assumed to be collimated arriving at 20°, this beam may, in fact, arrive at an angle slightly shifted by ±0.1°. Considering a one-dimensional angular distribution, the light arriving at the dichroic may consist of rays arriving at various angles. This paper studies the scenario of a beam with a one-dimensional angular distribution arriving at 20.1°.

## 3. RESULTS AND DISCUSSION

### 3.1 Modelling Optical Multilayer Coatings

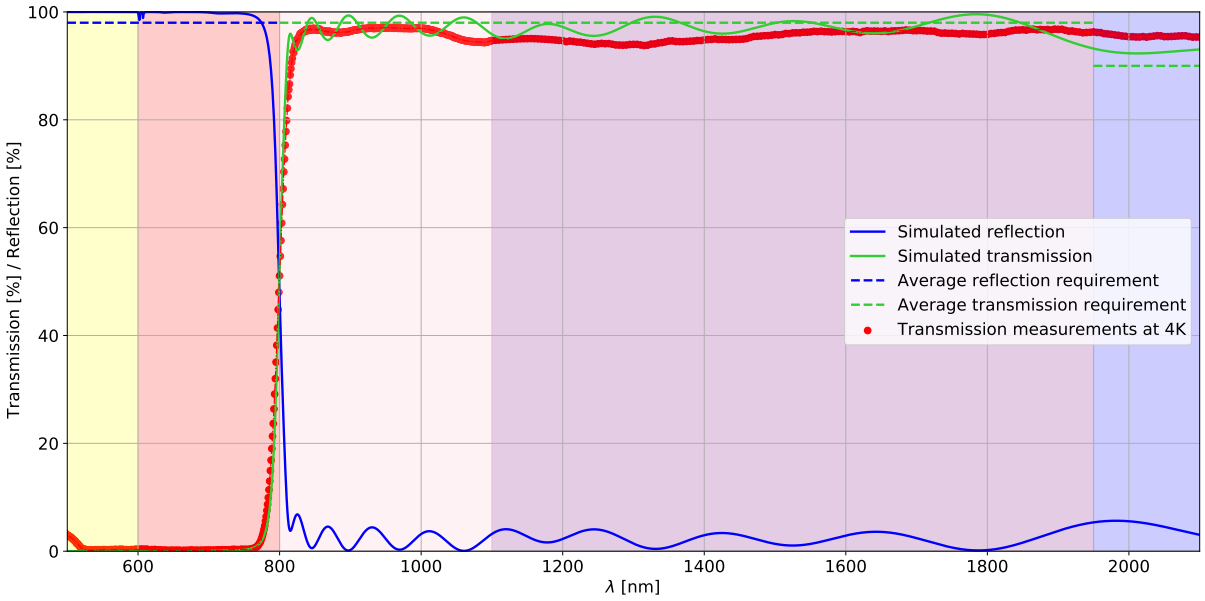


**Figure 2:** Spectral profile of the D3 design with a front and rear AR coating at 47.5K at an angle of incidence of 20°. Measurements of the D3 prototype performed have been plotted in red. The simulated transmission and reflection are represented as solid green and blue lines, respectively. The respective dashed lines indicate the required performance of D3 for a given waveband. The colored bands indicate the wavebands of various ARIEL channels. From left to right, these are VISPhot, FGS1, FGS2, NIRSpec, and AIRS-CH0.

The simulated overall reflection and transmission of D3 were modeled from an incident beam of light at a given angle at a multilayer structure composed of thin-film coating layers of specified thicknesses with given refractive indices. The coatings are bounded by a semi-infinite vacuum and an N-KB7 substrate on either surface. As D3 is known to have a rear AR coating, the performance of both the front and rear coatings were modeled individually. The overall reflection spectrum of the component is thus given by the sole reflection spectrum of the front coating, while the overall transmission spectrum is given by the product of the front and rear coating transmission spectra. An MC simulation was then conducted to make slight random variations of a few randomly chosen layers in the starting design, with the goal of optimizing the recipe to produce a reflectance spectrum in line with the requirements of D3.

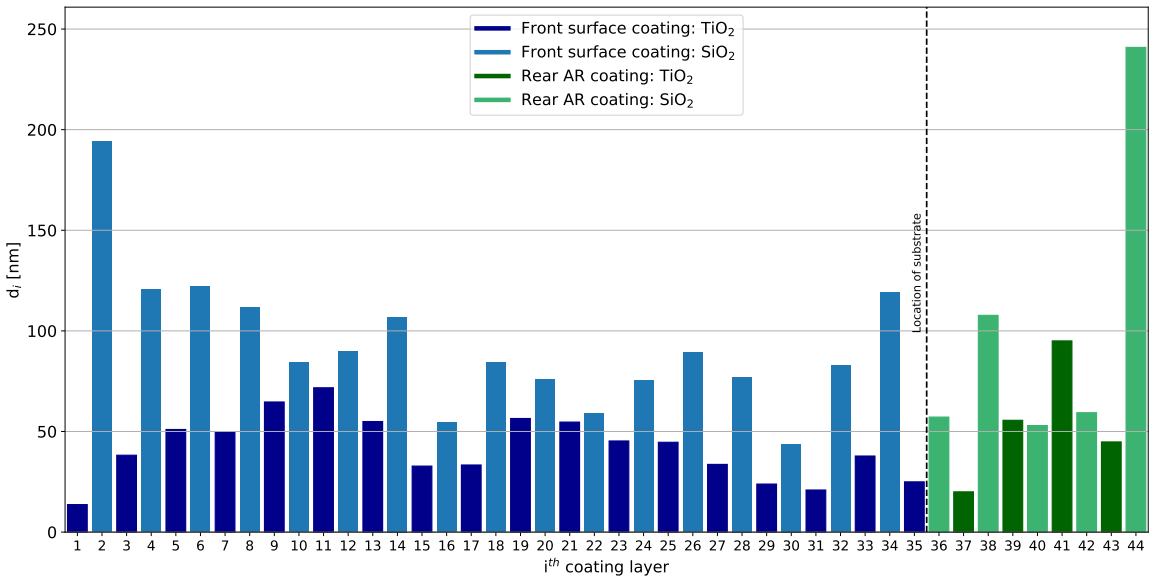


**Figure 3:** Thicknesses of individual coating layers, $d_i$, obtained from the optimization process. The blue bars indicate the thicknesses of the front surface coating layers, with $TiO_2$ and $SiO_2$ layers shown in dark and light blue. The thicknesses of the AR coating layers are shown as green bars, with $TiO_2$ and $SiO_2$ layers shown in dark and light green.

Fig. 2 shows the spectral profile of the optimised D3 design at 47.5K for an angle of incidence of 20° obtained from the MC simulation. The recipe, shown in Fig. 3, consists of alternating layers of $SiO_2$ and $TiO_2$, with a front coating of 35 layers and a rear AR coating of 9 coating layers, the thickness of each layer being a unique non-quarter-wave fractional thickness in order to reduce ripple amplitude. The design's simulated reflection, determined solely by the front coating of D3, meets and even exceeds the average reflection requirement of >98% for $500 < \lambda < 800$nm with 98.6%. The transition from the stopband to the passband also closely matches the measurements. The transition wavelength was found to be 799.48nm, occurring at the boundary between the FG1 and FGS2 channels by design. The simulated transmission of this D3 design also approximates the average transmission requirement of the component of >98% for $800 < \lambda < 1950$nm closely with a simulated average transmission of 96.9%. Moreover, the simulated average transmission within $1950 < \lambda < 2100$nm exceeds the requirement of >90%, with an average transmission of 92.6%.

### 3.2 Sources of Uncertainty

Several sources of uncertainty were modeled to illustrate their influence on the nominal performance of the D3 component and its multilayer coating.

Fig. 4 displays a contoured 2D histogram of the changes in performance resulting from 10,000 randomly generated errors on the thicknesses of all coating layers of ±0.5%. Each set of thicknesses generates a spectrum with a deviation in nominal performance, with 10,000 such deviations for each wavelength point. The plot shows a smooth vertical colorbar gradient centered near the $\Delta\tau = 0$ axis at all wavelengths. This indicates a Gaussian distribution of deviations in transmission centered around the nominal transmission of D3, suggesting a stable build with the performance of the dichroic remaining close to its nominal case, even in the presence of random deposition errors. Nonetheless, the enlarged portion of the contoured 2D histogram reveals the centers of the distributions that have been shifted narrowly beneath the $\Delta\tau = 0$ line. This is to be expected due to the optimization process in order to increase transmission in this region. Hence any errors or deviations from this optimized recipe will most likely yield a deterioration in performance and thus a decreased overall transmission.

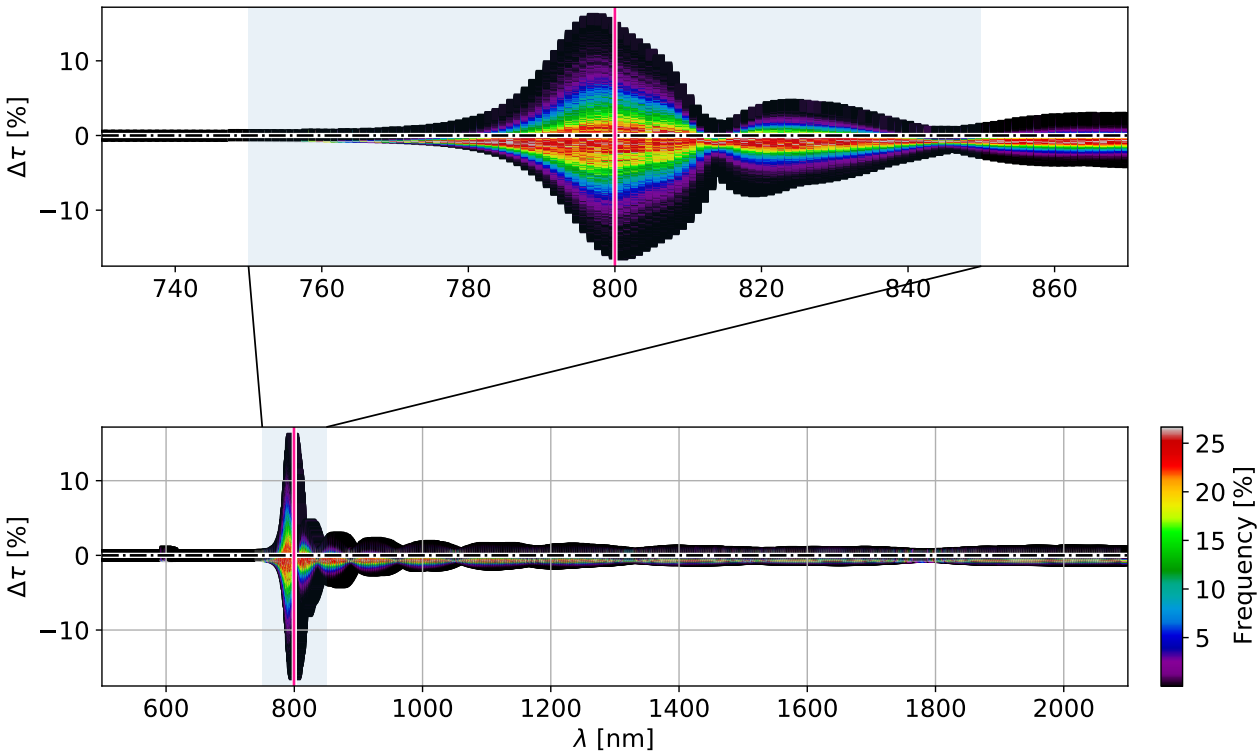


**Figure 4:** Deviation from nominal transmission due to random ±0.5% deposition errors in all coating layers of D3. Posterior distribution of the deviations from 10,000 randomly generated thickness errors on all layers as a contoured 2D histogram. The deviations at each wavelength are binned into bins of width $\Delta\tau = 0.1\%$, with the frequency percentage of the total 10,000 generated errors of each bin indicated by the colorbar. A dashed black line marks $\Delta\tau = 0$, and a solid pink line shows the nominal transition wavelength.

The deviations within the stopband remain insignificant due to the high performance of the coating in the wavelength region. However, the performance changes are significant within the majority of the passband, with higher deviations occurring at the wavelengths at which the ripples are present in Fig. 2. The most prominent deviations from the nominal transmission coincide with the transition wavelength region. As opposed to the regions of maximum transmission and reflection, where the primary objectives of a design are optical efficiency and an improvement in performance, the focus in the region of the transition is its exact location within the waveband. The deviation in the transmission of up to ±14.1% reveals the propensity of the transition wavelength to be shifted. Such a shift towards a lower wavelength than the nominal transition wavelength implies an increased transmission, whereas a shift to a higher wavelength results in a decreased transmission at the nominal transition wavelength.

The relative changes in the performance of our multilayer design of D3 resulting from each scenario are then applied directly to the measurements of a D3 prototype in order to assess the worst offenders to the optical performance. These results are shown in Fig. 5 and 6. A systematic coating layer thickness error in the form of a deficiency or surplus of 0.5% in all layers of the D3 coating resulted in a deviation near the transition wavelength of up to $\Delta\tau$=+17.5% at 797.0nm in the case of a deposition deficiency and $\Delta\tau$=-17.4% at 801.0nm for a deposition surplus, as displayed in Fig. 5. The significant number of coating layers leads to an increased design sensitivity to systematic thicknesses errors, thus inducing a shift in the positions of the transition to a lower and higher wavelength for the cases of deficiency and surplus, respectively. This procedure was repeated for the remaining parameters, as shown in Fig. 6 and 7. Similarly to the case for systematic deposition errors, the changes in transmission above 1$\mu$m remain inconsequential, with levels of $\Delta\tau$ <1% for all of these scenarios. The resultant deviations from the nominal reflectance for various other scenarios are presented in Fig. 6.

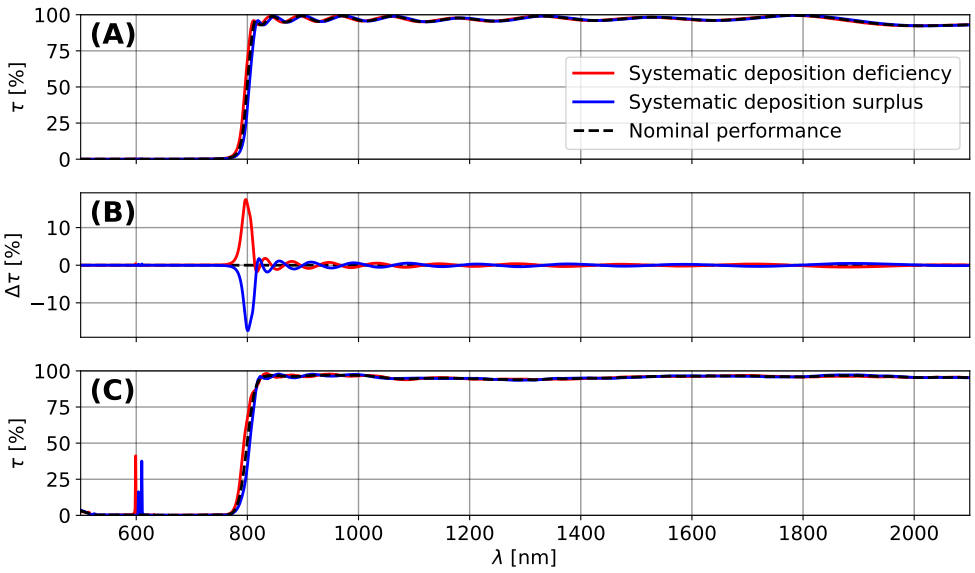


**Figure 5:** Change in the nominal transmission spectrum due to systematic deposition errors of 0.5% of each layer in all layers. The nominal performance is shown by a dashed black line, while the cases of systematic deposition deficiency and surplus are represented by red and blue lines, respectively. **(A)** transmission spectra resulting from changes in performance due to the systematic deposition errors. **(B)** Change in transmission from the nominal transmission of estimated D3 design. **(C)** Transmission spectra resulting from relative changes in nominal transmission of estimated D3 design caused by systematic thickness variations applied to the D3 prototype transmission spectrum measured at 4K.

In the case of a refractive index error, as a result of uncertainty in the knowledge of the $TiO_2$ index values, the most considerable deviation from the nominal transmission of $\Delta\tau$=3.0% occurs at 799.0nm. However, in comparison to the deviations from the nominal performance due to manufacturing uncertainties, the changes due to potential environmental changes during the operation of D3 in space are much lower in amplitude. The expected change in performance due to temperature fluctuations throughout an ARIEL observation is shown to be negligible, with a maximum variation of ±0.1%at 799.0nm. The maximum deviations on the spectral performance in the case of temperature offsets over the range of operating temperatures of D3 in space, displayed in Fig 7, were found to be $\Delta\tau$ <=-2.7% at 35K and $\Delta\tau$ <=2.6% at 60K both at 799.0nm. Moreover, the effect of an incident beam that arrives at 20.1°, rather than 20° had a negligible effect on the spectral performance of D3, with a maximum variation of 0.7% at 798.0nm, establishing that small changes in beam angles have an insignificant impact on the performance of D3.

### 3.2.1 Transition Wavelength Shifts

In order to further investigate these shifts in transition wavelength, the correlation of these shifts with each source of uncertainty was studied. A line was fitted to the slope of the transition section of the spectrum shown in Fig. 2, which was found to have a gradient of $4.54\text{nm}^{-1}$. This slope and its gradient, $m$, can be used to predict the shift in the transition wavelength using

$$m = \frac{\Delta\tau}{\Delta\lambda}, \tag{5}$$

where $\Delta\tau$ is the change in transmission observed at the nominal transition wavelength and $\Delta\lambda$ is the shift in the transition wavelength.

Thus,

$$\Delta\lambda = \frac{\tau_{unc} - 50\%}{m}, \tag{6}$$

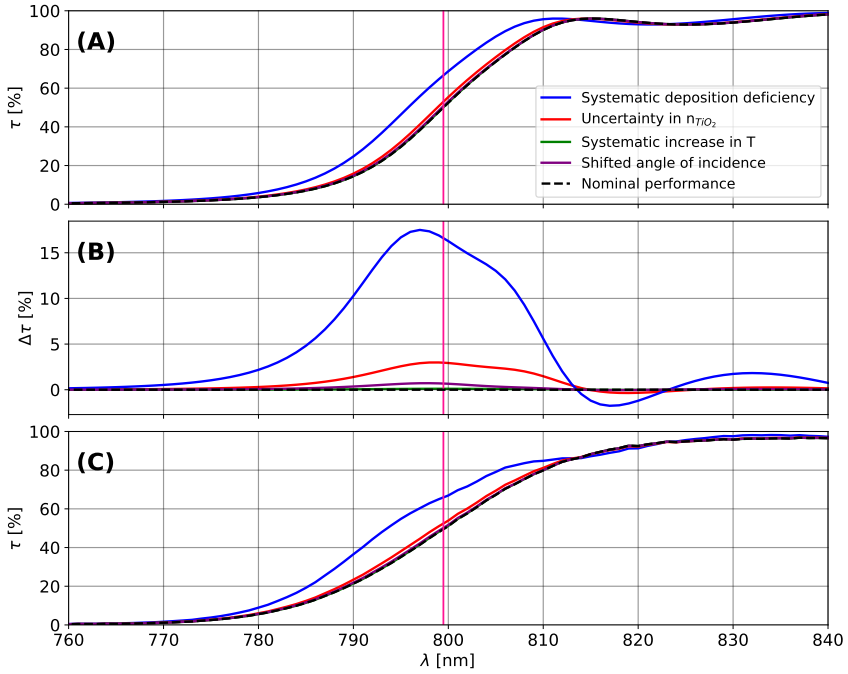


**Figure 6:** Change in the nominal transmission of D3 due to various changes in parameters. The nominal performance is shown by a dashed black line and the vertical pink line marks the transition wavelength of the nominal performance. The blue line shows the case of a -0.5% systematic thickness error in all coating layers. The red line indicates the scenario of a decrease of 0.1% in the refractive index of $TiO_2$ due to uncertainty in the knowledge of this value. The case of a +0.5K temperature offset is shown in green, with the performance at 47.5K taken to be the nominal transmission. The result of a beam shifted by +0.1° from the requirement of an angle of incidence of 20° is shown in purple. **(A)** Transmission spectra resulting from changes in performance due to each change in parameters. **(B)** Change in transmission from the nominal transmission of estimated D3 design. **(C)** Transmission spectra resulting from relative changes in nominal transmission of estimated D3 design caused by various systematic uncertainties applied to the D3 prototype transmission spectrum measured at 4K.

where $\tau_{unc}$ is the transmission at the nominal transition wavelength of the spectrum resulting from a given source of uncertainty. This shift in transition wavelength can be calculated directly using Eq(6) for all scenarios for which we obtain a single spectrum. However, for the case of random thicknesses errors in all coating layers, we generate 10,000 random errors and thus 10,000 individual spectra. In this case, the distribution of $\Delta\tau$ at the nominal transition wavelength was found. Fig. 4 indicates that this distribution resembles a Gaussian distribution, and thus, a Gaussian curve was fitted to it. The standard deviation of this fit informs us of the standard possibility of a given transmission at the expected transition wavelength, and so, this value was used to represent $\Delta\tau$ in Eq(5).

The results of this investigation are shown in Fig. 8. The shift in transition wavelength correlates linearly with each source of uncertainty. Coating layer thickness errors and uncertainty in refractive index show a positive correlation, while a negative correlation is observed for the offsets in temperature and angle of incidence. The amplitude of $\Delta\tau$ in Fig. 6 directly corresponds with the shift in transition wavelength predicted in Fig. 8. This can be most clearly seen with the case of systematic layer thickness errors, for which shifts in the transition wavelength ranging from -4.32nm to +4.42nm are displayed in Fig. 8. For a systematic deposition deficiency of 0.5% on all coating layers, a transition wavelength shift of -4.32nm has been predicted, thus placing the new transition wavelength at 795.16nm. Comparing this to Fig. 6, this prediction agrees with the high change in transmission observed at this wavelength.

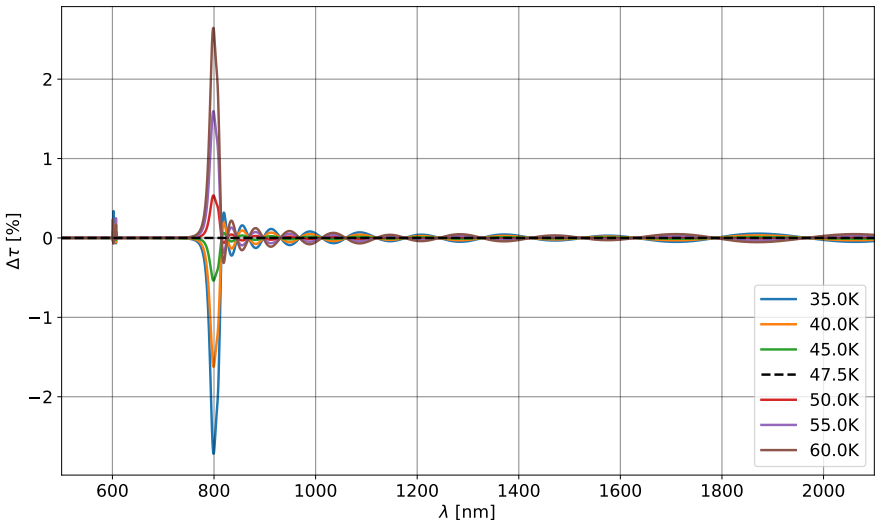


**Figure 7:** Deviation from the nominal transmission at various temperature offsets within the predicted operating range of D3 with the transmission spectrum at 47.5K is taken to be the nominal performance.

### 3.3 Limitations

A number of limitations of the model must be considered. One such limitation is that the accuracy of this model is restricted by the accuracy of the parameter models provided. The temperature dependence of the index of refraction of N-KB7 and $TiO_2$ at the required cryogenic temperatures has not been published in any literature currently known to the authors. In order to address this limitation, the closest available temperature-dependent models of the indices were linearly extrapolated to 47.5K for the simulation of the nominal performance of D3. For the case of N-KB7, the refractive index model applies at 50K-300K, so a linear interpolation to 47.5K is not far outside this temperature range. Additionally, the refractive index of the material is shown to have a weak temperature dependence, with virtually no change in $n(\lambda)$ at 50K and 300K, as can be seen in Fig. 9. Thus, a linear extrapolation of the model to lower cryogenic temperatures is a reasonable approximation. However, for $TiO_2$, only a temperature-dependent model of the refractive index down 303.15K for $454nm < \lambda < 1300nm$ is known to the authors. In comparison to N-KB7, this model shows a stronger temperature dependence, notably at higher wavelengths. A linear extrapolation to higher wavelengths is a potentially suitable extension of this model due to the weak power-law dependence $TiO_2$ has been shown to follow for $430nm < \lambda < 1530nm$.[35] Nonetheless, a linear extrapolation to cryogenic temperatures from such high temperatures may not be ideal, being so far from the verified temperature ranges of this model. This matter warrants further investigation into cryogenic indices of $TiO_2$ in particular.

A further assumption is a negligible effect of temperature regarding the thermal expansion of the materials, which in turn affects the thicknesses of the layers. If temperature changes in space severely modify thicknesses, this must be considered. However, in this case, the order of expected operational temperature changes is considered minor. Thus the temperature coefficients of linear expansion are significantly smaller in value compared to the temperature coefficients of the refractive indices. Thus, changes in performance due to the temperature variations are dominated by the variation these cause in the refractive indices.[9]

Moreover, a potentially significant limitation of this model is the assumption that the coating layers are entirely uniform. The D3 coating consisting of a considerable number of layers will likely result in scattering due to the increased risk of non-uniformities at the interfaces of these layers, particularly at non-normal incidence. This model does not take into account losses due to the surface roughness and resultant scattering. This effect is usually of the order of a few nm per optical surface, thus resulting in a more significant impact on multilayer structures with a significant number of coating layers. In addition to scattering effects due to a significant roughness at the layer interfaces,[36] the impact of shallow roughness features that occur naturally in a thin film

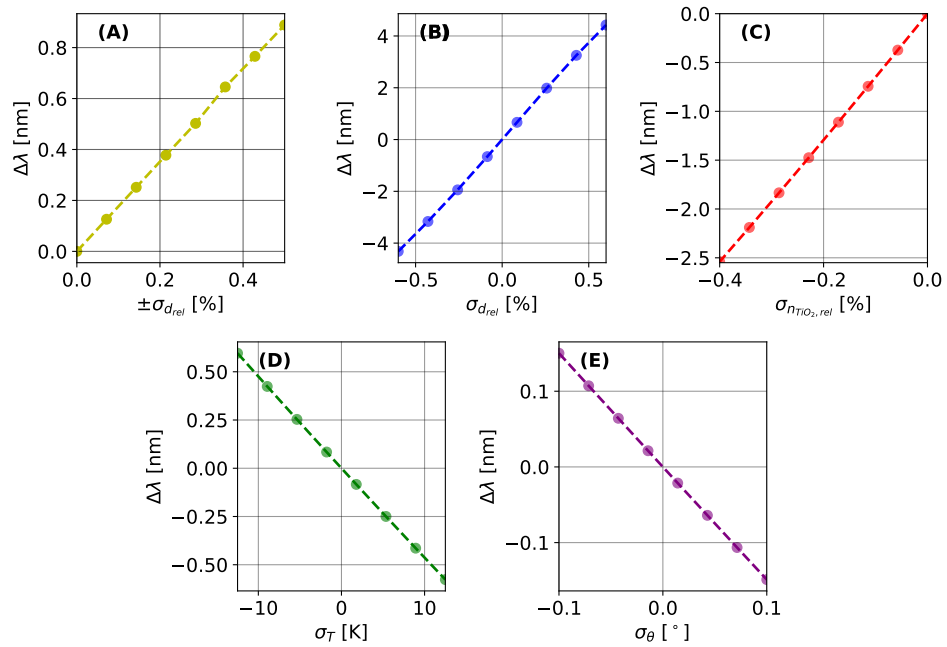


**Figure 8:** Shift in transition wavelength due to each scenario. Plots **(A)** and **(B)** represent the transition wavelength shifts found for a range of relative multilayer coating thickness errors for the cases of random and systematic errors in all layers, respectively. **(C)**,**(D)** and **(E)** show the scenarios of a range of relative uncertainties in the knowledge of the refractive index of $TiO_2$, temperature offsets from the nominal average operating temperature of 47.5K and a variation in the angle of incidence from the nominal angle of 20°, respectively.

due to its microstructure may need to be included in this model in the future.[37] Moreover, the significance of losses due to multiple internal cavity reflections as a result of this roughness should also be investigated further.[9]

## 4. CONCLUSION

Using this model, we are able to predict the levels of uncertainty in the performance of a multilayer system. This paper explores the application of this model to the Ariel dichroic beamsplitter D3 in order to investigate the tolerance of this dichroic to uncertainties that may affect its optical performance. Various systematics may result in the shifting of the transition wavelength of the dichroic beamsplitter. Uncertainties in the thicknesses of the coating layers and uncertainty in the index of refraction may be the worst offenders to the performance of a dichroic and the designed position of the transition wavelength. On the other hand, temperature and angle of incidence offsets are likely only to have a minor effect on the expected performance. The uncertainties outlined here must be taken into consideration in order to achieve the desired performance of this multilayer system. Combinations of any number of such sources of uncertainty may be combined with increasing model complexity. Statistical information obtained from a number of these simulations can be used as a basis to establish the performance stability of the component. This will provide a better understanding of deviations from the nominal simulated performance observed during measurements of the component observed during the testing process, both due to the build and any optical effects.

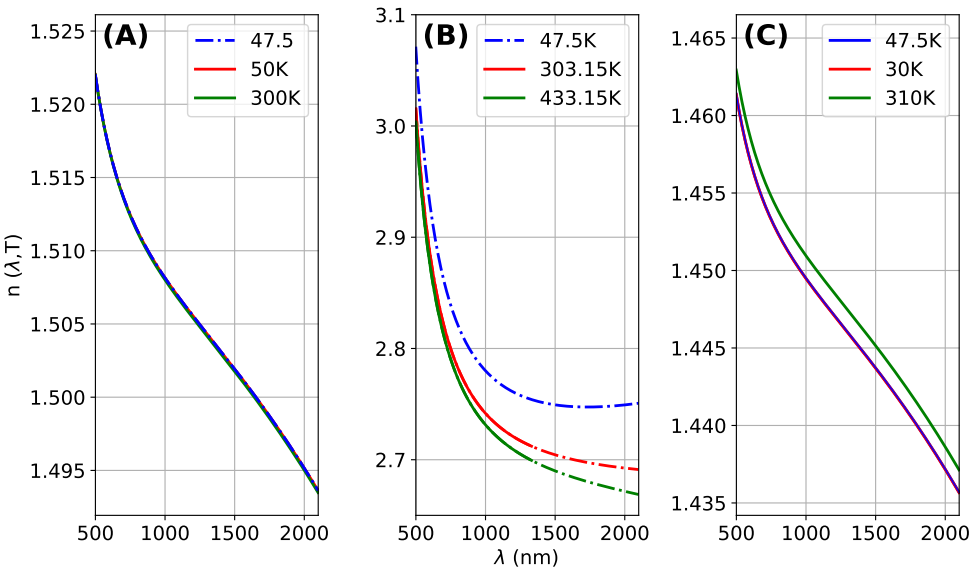


**Figure 9:**
Temperature-dependent models of the refractive indices of the assumed D3 materials as a function of the D3 waveband. Plots **(A)**, **(B)** and **(C)** represent the materials N-KB7, $TiO_2$ and $SiO_2$ respectively. Solid lines represent values calculated directly from each model within the temperature and wavebands for which the model has been confirmed. Dashed lines indicate extrapolated values of the confirmed models to temperatures or wavelengths outside of the confirmed ranges. The indices at the average operating temperature of ARIEL (47.5K) has been plotted in blue, whereas the indices at the minimum and maximum temperatures for which each model has been confirmed, are shown in red and green, respectively.

## REFERENCES


[1] Tinetti, G., Drossart, P., Eccleston, P., Hartogh, P., Heske, A., Leconte, J., Micela, G., Ollivier, M., Pilbratt, G., Puig, L., et al., "The science of ariel (atmospheric remote-sensing infrared exoplanet large-survey)," in [*Space Telescopes and Instrumentation 2016: Optical, Infrared, and Millimeter Wave*], **9904**, 99041X, International Society for Optics and Photonics (2016).

[2] Tinetti, G., Eccleston, P., Haswell, C., Lagage, P.-O., Leconte, J., Lüftinger, T., Micela, G., Min, M., Pilbratt, G., Puig, L., et al., "Ariel: Enabling planetary science across light-years," *arXiv preprint arXiv:2104.04824* (2021).

[3] Da Deppo, V., Focardi, M., Morgante, G., Middleton, K., Pace, E., Claudi, R., and Micela, G., "The optical configuration of the telescope for the ariel esa mission," in [*Space Telescopes and Instrumentation 2018: Optical, Infrared, and Millimeter Wave*], **10698**, 106984O, International Society for Optics and Photonics (2018).

[4] Pascale, E., Eccleston, P., and Tinetti, G., "The ariel space mission," in [*2018 5th IEEE International Workshop on Metrology for AeroSpace (MetroAeroSpace)*], 31–34, IEEE (2018).

[5] Rataj, M., Wawer, P., Skup, K., and Sobiecki, M., "Design of fine guidance system (fgs) for ariel mission," in [*Photonics Applications in Astronomy, Communications, Industry, and High-Energy Physics Experiments 2019*], **11176**, 1007–1013, SPIE (2019).

[6] Hawkins, G. and Hunneman, R., "A spectral performance model for the high resolution dynamics limb sounder (6–18 $\mu$m)," *Infrared physics & technology* **41**(4), 239–246 (2000).

[7] Hawkins, G. J., Hunneman, R., Sherwood, R., and Barrett, B. M., "Infrared filters and coatings for the high resolution dynamics limb sounder (6–18 $\mu$m)," *Applied optics* **39**(28), 5221–5230 (2000).

[8] Hawkins, G. and Sherwood, R., "Cooled infrared filters and dichroics for the james webb space telescope mid-infrared instrument," *Applied optics* **47**(13), C25–C34 (2008).

[9] Hawkins, G., Sherwood, R., and Djotni, K., "Mid-infrared filters for astronomical and remote sensing instrumentation," in [*Advances in Optical Thin Films III*], **7101**, 710114, International Society for Optics and Photonics (2008).

[10] Dupoisot, H. and Morizet, J., "Thin film coatings: algorithms for the determination of reflectance and transmittance, and their derivatives," *Applied optics* **18**(15), 2701–2704 (1979).

[11] Baumeister, P., "Optical interference coatings," *Applied optics* **15**(10), 2313–2314 (1976).

[12] Orfanidis, S. J., "Electromagnetic waves and antennas, 2008," *Unpublished, available: http://www. ece. rutgers. edu/orfanidi/ewa* (2004).

[13] Dobrowolski, J. and Kemp, R., "Refinement of optical multilayer systems with different optimization procedures," *Applied optics* **29**(19), 2876–2893 (1990).

[14] Sullivan, B. T. and Dobrowolski, J. A., "Deposition of metal/dielectric multilayer filters," in [*Optical Interference Coatings*], **2253**, 1213–1217, International Society for Optics and Photonics (1994).

[15] Dirks, A. and Leamy, H., "Columnar microstructure in vapor-deposited thin films," *Thin solid films* **47**(3), 219–233 (1977).

[16] Flory, F., Borgogno, J.-P., Endelema, D., Rausa, E., Rigneault, H., and Rizzo, A., "Interpreting anisotropy and disturbances of optical properties of thin films in terms of layer microstructure," in [*Optical Interference Coatings*], **2253**, 1232–1242, International Society for Optics and Photonics (1994).

[17] Bauer, H. H. and Nuessler, E., "In situ optical multichannel spectrometer system," in [*Optical Interference Coatings*], **2253**, 423–431, International Society for Optics and Photonics (1994).

[18] Sullivan, B. T. and Dobrowolski, J., "Deposition error compensation for optical multilayer coatings. i. theoretical description," *Applied optics* **31**(19), 3821–3835 (1992).

[19] Hawkins, G. and Hunneman, R., "The temperature-dependent spectral properties of filter substrate materials in the far-infrared (6–40 $\mu$m)," *Infrared physics & technology* **45**(1), 69–79 (2004).

[20] Morgante, G., Terenzi, L., D'Ascanio, D., Eccleston, P., Crook, M., Hunt, T., Da Deppo, V., Focardi, M., Malaguti, G., Micela, G., et al., "Thermal architecture of the esa ariel payload," in [*Space Telescopes and Instrumentation 2018: Optical, Infrared, and Millimeter Wave*], **10698**, 106984H, International Society for Optics and Photonics (2018).

[21] Sørensen, B. F., Sarraute, S., Jørgensen, O., and Horsewell, A., "Thermally induced delamination of multilayers," *Acta materialia* **46**(8), 2603–2615 (1998).

[22] Wang, X., Masumoto, H., Someno, Y., and Hirai, T., "Helicon plasma deposition of a tio 2/sio 2 multilayer optical filter with graded refractive index profiles," *Applied physics letters* **72**(25), 3264–3266 (1998).

[23] Yao, J., Shao, J., He, H., and Fan, Z., "Effects of annealing on laser-induced damage threshold of tio2/sio2 high reflectors," *Applied Surface Science* **253**(22), 8911–8914 (2007).

[24] Jena, S., Tokas, R., Thakur, S., and Sahoo, N., "Influence of annealing on optical, microstructural and laser induced damage properties of tio2/sio2 multilayer high reflection mirror," in [*AIP Conference Proceedings*], **1832**(1), 060005, AIP Publishing LLC (2017).

[25] Frey, B. J., Leviton, D. B., Madison, T. J., Gong, Q., and Tecza, M., "Cryogenic temperature-dependent refractive index measurements of n-bk7, balkn3, sf15, and e-sf03," in [*Cryogenic Optical Systems and Instruments XII*], **6692**, 31–42, SPIE (2007).

[26] Rams, J., Tejeda, A., and Cabrera, J., "Refractive indices of rutile as a function of temperature and wavelength," *Journal of Applied Physics* **82**(3), 994–997 (1997).

[27] Leviton, D. B. and Frey, B. J., "Temperature-dependent absolute refractive index measurements of synthetic fused silica," in [*Optomechanical Technologies for Astronomy*], **6273**, 62732K, International Society for Optics and Photonics (2006).

[28] Wells, M., Hawkins, G., and Olofsson, G., "The design and fabrication of multiple dichroic beamsplitters for the miri spectrometer (4.8-29$\mu$m)," in [*Optical, Infrared, and Millimeter Space Telescopes*], **5487**, 794–803, International Society for Optics and Photonics (2004).

[29] Kischkat, J., Peters, S., Gruska, B., Semtsiv, M., Chashnikova, M., Klinkmüller, M., Fedosenko, O., Machulik, S., Aleksandrova, A., Monastyrskyi, G., et al., "Mid-infrared optical properties of thin films of aluminum oxide, titanium dioxide, silicon dioxide, aluminum nitride, and silicon nitride," *Applied optics* **51**(28), 6789–6798 (2012).

[30] Siefke, T., Kroker, S., Pfeiffer, K., Puffky, O., Dietrich, K., Franta, D., Ohlídal, I., Szeghalmi, A., Kley, E.-B., and Tünnermann, A., "Materials pushing the application limits of wire grid polarizers further into the deep ultraviolet spectral range," *Advanced Optical Materials* **4**(11), 1780–1786 (2016).

[31] Gao, L., Lemarchand, F., and Lequime, M., "Refractive index determination of sio2 layer in the uv/vis/nir range: spectrophotometric reverse engineering on single and bi-layer designs," (2013).

[32] SCHOTT, "SCHOTT Zemax catalog 2017-01-20b." Available online: http://refractiveindex.info/download/data/2017/schott_2017-01-20b.agf. (Accessed on 13 June 2022).

[33] Ribeaud, A., Pistner, J., Hagedorn, H., and Joseph, S., "Infra-red multi-layer coatings using ybf3 and zns in an ion beam sputtering system," in [*Optical Interference Coatings*], MC–7, Optical Society of America (2019).

[34] Morgante, G., Terenzi, L., Desjonqueres, L., Eccleston, P., Bishop, G., Caldwell, A., Crook, M., Drummond, R., Hills, M., Hunt, T., et al., "The thermal architecture of the esa ariel payload at the end of phase b1," *Experimental Astronomy* , 1–40 (2022).

[35] D. Shannon, R., Shannon, R. C., Medenbach, O., and Fischer, R. X., "Refractive index and dispersion of fluorides and oxides," *Journal of physical and chemical reference data* **31**(4), 931–970 (2002).

[36] Roennow, D. and Roos, A., "Optical characterization of interface roughness of thin films on transparent substrates," in [*Optical Interference Coatings*], **2253**, 1050–1059, International Society for Optics and Photonics (1994).

[37] Garcia-Llamas, R. and Regalado, L. E., "Effects of rough interfaces in a multilayer stack," in [*Optical Interference Coatings*], **2253**, 1298–1312, International Society for Optics and Photonics (1994).